Thin-Walled Structures 182 (2023) 110231

Contents lists available at ScienceDirect

Thin-Walled Structures

journal homepage: www.elsevier.com/locate/tws

Full length article

Semi-analytical study of buckling response for grid-stiffened panels during creep age forming

Wenbin Zhou, Zhusheng Shi *, Jianguo Lin

Department of Mechanical Engineering, Imperial College London, London SW7 2AZ, UK

ARTICLE INFO

Keywords:
Stiffened panel
Elastic–plastic buckling
Creep age forming
Bending load
Effective width
Plasticity theory

ABSTRACT

The elastic–plastic buckling response of panels with grid stiffeners during creep age forming (CAF) has been studied using a semi-analytical method in this research. A simplified model for panels with multiple grid stiffeners under bending has been established and the effective width has been applied to consider the flexible skin effect and multiple stiffener effect. In the semi-analytical method, the equilibrium equation for the simplified model has been solved via differential quadrature method to acquire the buckling stress of grid-stiffened panels, using deformation theory (DT) and incremental theory (IT) of plasticity. The results with IT show good agreements with both the published experimental and non-linear FE results, demonstrating its effectiveness. Based on the method, the effects of geometric dimensions of grid-stiffened panels, multiple stiffeners and temperature on buckling response in the elastic and plastic regions have been studied. It is found that the transverse stiffener provides a 13.9% higher buckling stress of grid-stiffened panels than blade-stiffened panels, and buckling may occur in the heating stage during CAF. The proposed semi-analytical method based on IT provides accurate predictions of buckling stress during either CAF or cold forming, which can guide the parameter optimisation of grid-stiffened panels in design.

1. Introduction

Integrally stiffened panels are the main loading structure in aerospace industries to achieve lightweight for transportation [1,2]. Creep age forming (CAF), an advanced metal forming technology for manufacturing large aluminium alloy workpieces, combines forming and ageing heat treatment in a single process to manufacture the components [3]. CAF has been considered as a highly potential forming technology to manufacture integrally grid-stiffened panels with low residual stress, high strength and high process repeatability [4,5]. The principal procedure of CAF process includes three main operations: loading, creep-ageing and unloading. In the loading stage of CAF, the stiffened panel is placed in the forming dies and loaded at room temperature. The stiffened panel with the dies is then moved in the oven to heat and kept at the ageing temperature for the required time, during which creep strain generates and the stiffened panel is deformed [6]. Bending is the general loading condition in the CAF process.

The challenge arises for the forming of the integrally stiffened panel since the skin and the stiffener will be formed together under bending in the forming process, in which the stiffener is subjected to relatively large stress which may cause damage or buckling to the stiffener [7,8]. The buckling issue in the forming process is a constraint that need be considered in the geometry optimisation of stiffened panels in design. Non-linear Finite Element (FE) and experimental investigations have been implemented to acquire buckling responses of stiffened panels during CAF process, and the prediction error of the non-linear FE method is within 6.3% compared with experimental results of stiffened panels with the corresponding geometry [9,10]. Recently, novel machine learning-driven method has been applied in the buckling analysis, greatly accelerating the efficiency [11,12]. However, non-linear FE simulations lead to an extremely long total calculation time for the design of stiffened panels due to the iteration process required in the parameter optimisation [13]. Therefore, it is significant to develop an analytical or semi-analytical method for buckling analysis of grid-stiffened panels during the CAF with bending loads, which can obtain reliable results in a low time-consuming manner to predict the forming limit in CAF and cold forming [14].

Buckling response of stiffened panels with blade stiffener has been analysed under uniform compression [13,15] and bending [16,17] using equilibrium method with the prediction error of 5.8%. In these cases, simplified models for stiffened panels with single blade stiffener have been proposed, which is a plate (skin for uniform compression condition and stiffener for bending condition) adding an elastically built-in (EBI) boundary condition for the rotation constraint on the bottom edge between the blade stiffener and the skin to account for their interaction effect [13,16]. An effective width has been proposed

* Corresponding author.
E-mail address: zhusheng.shi@imperial.ac.uk (Z. Shi).

https://doi.org/10.1016/j.tws.2022.110231
Received 17 June 2022; Received in revised form 11 September 2022; Accepted 6 October 2022
Available online xxxx
0263-8231/© 2022 The Author(s). Published by Elsevier Ltd. This is an open access article under the CC BY license (http://creativecommons.org/licenses/by/4.0/).

Nomenclature

$[A]$, $[B]$	Matrices of deflection and buckling stress in generalised eigenvalue equations respectively (–)
a	Length of stiffened panel (mm)
b, b_{eff}	Width and effective width of stiffened panel (mm)
E, E_t, E_s	Young's modulus, tangent modulus and secant modulus (GPa)
F_X	Applied normal force of stiffened panel per unit length in the x-direction (N/m)
G	Shear modulus (GPa)
h	Stiffener height (mm)
k_t, m_t	Yield offset and reciprocal of strain hardening exponent (–)
k_{cr}	Critical buckling coefficient (–)
M_{yy}, M_{xy}	Moment per unit length respectively from σ_{yy} and σ_{xy} ((N m)/m)
M_b, M_l	Moments per unit length applied on bottom edge and loading edge of longitudinal stiffener respectively by skin and transverse stiffener, which act as bending moments ((N m)/m^{-1})
M_b', M_l'	Moments per unit length applied on skin and transverse stiffener respectively by bottom edge and loading edge of longitudinal stiffener, which act as torsional moments ((N m)/m^{-1})
M_{b0}'	Moment per unit length at middle of bottom edge in x-direction ((N m)/m^{-1})
M_z	Applied moment in z-direction on stiffened panel (N m)
m	Number of sinusoidal half-waves in x-direction (–)
N	Number of grid points (–)
Q_{yz}	Resultant shearing force per unit length in the yz-planes (N/m)
t_{sk}, t_{st}	Skin thickness and stiffener thickness (mm)
U_x, U_y, U_z	Translations in x-, y- and z-directions (mm)
UR_x, UR_y, UR_z	Rotation about x-, y- and z-axes (–)
u, v, w	Deflections of transverse stiffener in x-direction, skin in y-direction and longitudinal stiffener in z-direction (mm)
y_0	Distance between bottom of longitudinal stiffener and neutral plane of stiffened panel (mm)
α, β, γ	Material constants for incremental and deformation theories of plasticity (–)
ε, ε_{ij}	Strain and strain components (–)
κ^2	Shear correction factor (–)
ν	Poisson's ratio (–)
σ, σ_{ij}	Stress and stress components (MPa)
σ_b	Buckling stress (MPa)
σ_0	Offset yield stress (MPa)
ϕ_x, ϕ_y	Rotation angles of longitudinal stiffener about the y- and x-axis (rad)
$\phi_y^{f'}$, $\phi_y^{r'}$	Rotation angles of flexible skin/rigid skin about x-axis (rad)
ΔX, $\dot{X}$	Increment and time derivative of variable X respectively ($[X]$, $[X]$/s)

to consider the influence of the flexible skin with free boundary condition on the buckling of single-stiffener blade-stiffened panel loaded by bending [16]. In the equilibrium method, the equilibrium equations based on Kirchhoff–Love plate theory (thin plate bending theory) [18] or the Mindlin–Reissner plate theory (thick plate bending theory) [19] considering the first-order shear effect through the thickness of the plate are solved to predict the buckling stress.

In the plastic buckling analysis, two main plasticity theories have been applied to predict the buckling stress of different structures considering the non-linear material property, such as plates [20,21] and stiffened panels [22]. These two theories are incremental theory (IT) based on Prandtl–Reuss constitutive equations and deformation theory (DT) based on the Hencky equations. The strain in IT is dependent on the whole path of stress, while the total strain in DT is only related to the certain stress [23,24]. Several investigations have revealed that DT generally predicts a lower buckling stress compared with IT [21,25]. The stress distribution in components under plastic bending covers the elastic and plastic regions. The equilibrium equations with varying material constants in the buckling analysis can be solved using the differential quadrature (DQ) method [17].

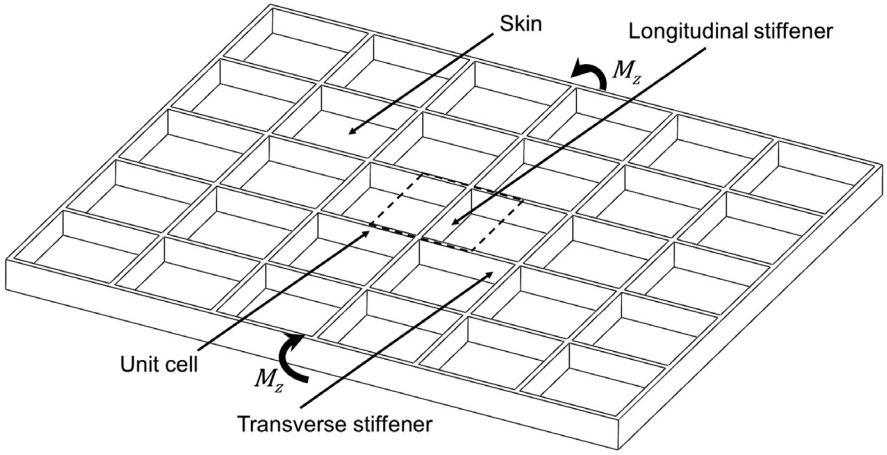
Global and local buckling response of grid-stiffened panels has been investigated subjected to axial compression [26–28] and shear loading [29], in which both skin buckling and stiffener crippling were the buckling mode. The results showed that the presence of stiffeners increased the elastic buckling stress of the local skin between stiffeners. The buckling analysis of grid-stiffened cylinder loading by axial compression has been conducted with different grid patterns, including orthogrid [30], isogrid [31,32], and triangle grid [33]. In addition, material properties will change when the temperature is increased from the room temperature to the ageing temperature, leading to the difference of buckling behaviour under different temperatures. However, no report has been found on studies of elastic–plastic buckling response of grid-stiffened panels loaded by bending analytically for forming process and in heating conditions.

A semi-analytical method, based on Mindlin–Reissner plate theory, is developed in this study for grid-stiffened panels in CAF process. The EBI boundary condition and the effective width are introduced in the simplified model of grid-stiffened panel to consider the influence of flexible skin and transverse stiffeners. The semi-analytical method is used to predict the buckling results of grid-stiffened panels loaded by bending, and the predictions are compared with the corresponding experimental results and non-linear FE results. In addition, the effects of the geometric parameters, multiple stiffeners and temperature on the buckling response have been studied based on the semi-analytical and non-linear FE methods.

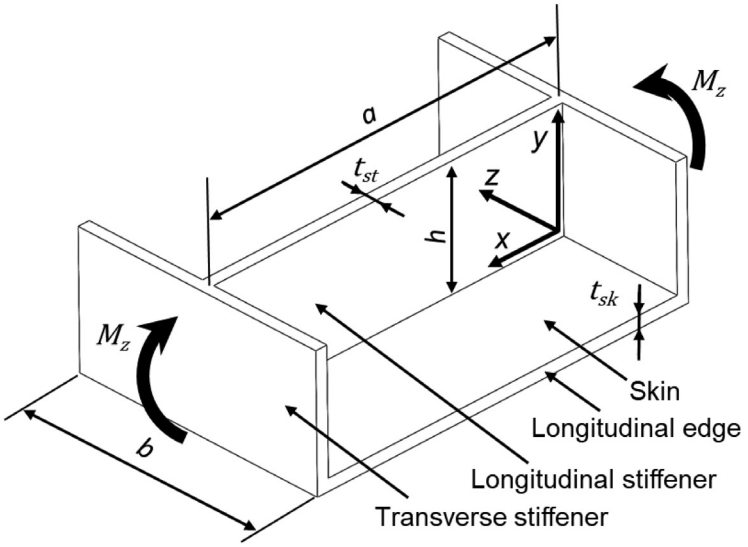
2. Simplified model of grid-stiffened panel

2.1. Problem definition

The object of buckling analysis in this research is grid-stiffened panels under bending moment M_z, as presented in Fig. 1(a). A unit cell of the continuous grid-stiffened panel can be captured from the dashed rectangle in Fig. 1(a), which has two transverse blade stiffeners and one longitudinal blade stiffener. The geometric parameters of the unit cell include stiffened panel length (longitudinal stiffener length between adjacent transverse stiffeners) a, stiffened panel width (transverse stiffener length between adjacent longitudinal stiffeners) b, stiffener thickness t_{st}, skin thickness t_{sk} and stiffener height h, as shown in Fig. 1(b). Two longitudinal edges of the unit cell are treated as free for single-stiffener condition, but have symmetric or antisymmetric



(a) Grid-stiffened panel



(b) Unit cell

Fig. 1. Schematic showing grid-stiffened panel subjected to bending.

boundary condition for multi-stiffener condition [34,35]. The Mindlin–Reissner theory is applied in the buckling investigation to account for the first-order shear effect. The buckling behaviour for grid-stiffened panels with the single-stiffener and the multi-stiffener conditions will be investigated using the unit cell.

2.2. Buckling mode and buckling model

During CAF of stiffened panels, the skin is generally in tension and the stiffener in compression during loading; thus, only stiffener buckling mode takes place on grid-stiffened panels under bending, where large deflection occurs on the top of longitudinal stiffener due to large compression during forming [10]. Fig. 2(a) schematically shows the stiffener buckling mode of grid-stiffened panels, where w, u and v are the deflections of the longitudinal stiffener in z-direction, the transverse stiffeners in x-direction and the skin in y-direction, respectively, and ϕ_x and ϕ_y represent rotation angles of longitudinal stiffener about y-axis and x-axis respectively.

To investigate the influence of the transverse stiffener and skin on the buckling occurring on longitudinal stiffener, the internal force of longitudinal stiffener, transverse stiffener and skin regions of grid-stiffened panels are presented in Fig. 2(b)–(d). For the longitudinal stiffener in Fig. 2(b), the constraints from the transverse stiffener and skin which can be instead of M_l at two loading edges and bending moments M_b at the bottom edge, respectively. In addition, the transverse stiffener and skin are subjected to an equivalent reaction torsional moment M_l' along the loading edge (Fig. 2(c)) and an equivalent reaction torsional moment M_b' along the bottom edge (Fig. 2(d)), respectively.

A simplified model for the grid-stiffened panels loaded by bending is developed from the previous simplified model for blade-stiffened panels in [16,17]. In the model of grid-stiffened panels, EBI boundary conditions are set on the two loading edges and the bottom edge of longitudinal stiffener to consider the rotational constraints from the transverse stiffeners and the skin (M_l' in Fig. 2(c) and M_b' in Fig. 2(d)), as shown in Fig. 3. The upper edge of the simplified model is free.

In the EBI boundary condition of the bottom edge and loading edge, the displacements in z-direction are both fixed, the rotation in

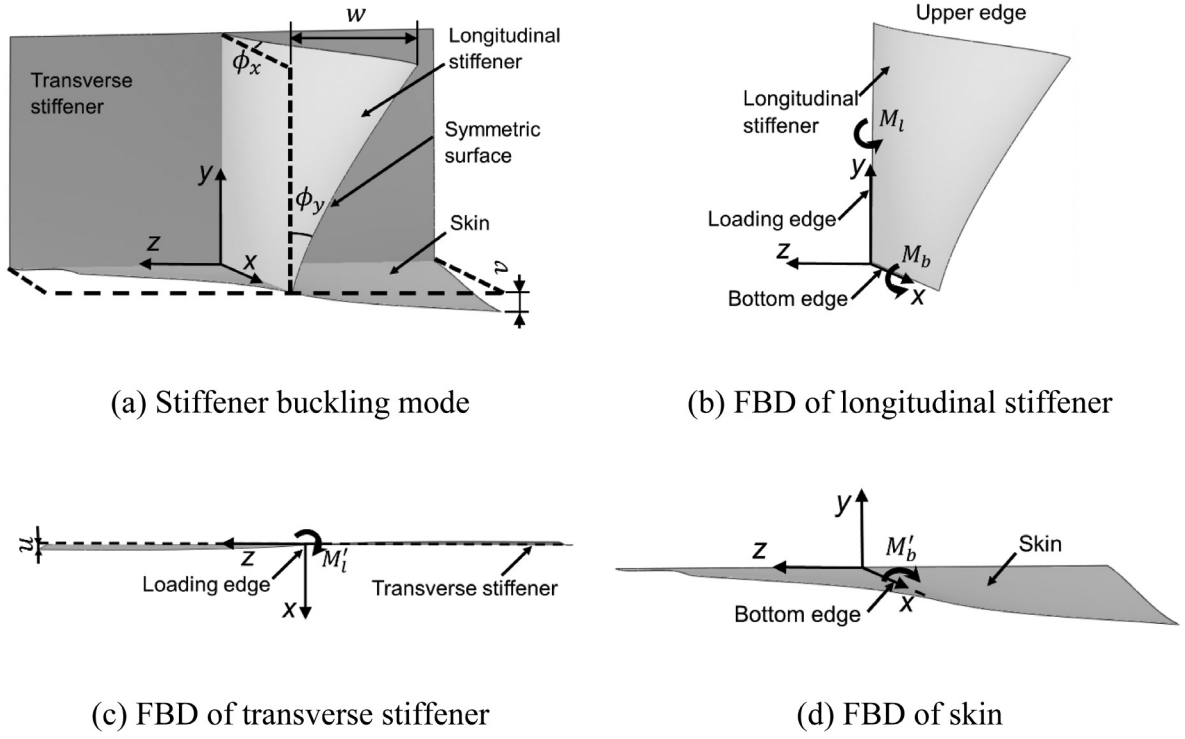


Fig. 2. Buckling mode of grid-stiffened panel loaded in bending and breakdown free body diagrams (FBD) of longitudinal and transverse stiffeners and skin. Note that (c) is viewed from positive y-direction to show xz-plane.

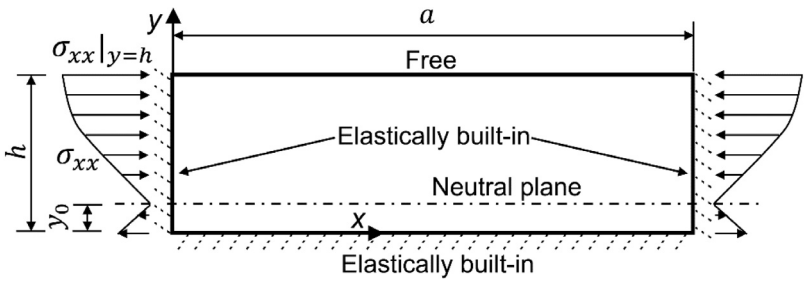


Fig. 3. Simplified model of grid-stiffened panels loaded by plastic bending moment for buckling analysis.

x-direction of the bottom edge is restricted by M_b' and the rotation in y-direction of the loading edge is restricted by M_l'. The rotational constraints of the EBI boundary conditions are defined by $M_b + M_b' = 0$ along the bottom edge and $M_l + M_l' = 0$ along the loading edge.

2.3. Stress distribution

The stress distribution in the unit grid-stiffened panel under bending which is simplified to that of blade-stiffened panel ignoring the effect of the transverse stiffener is briefly introduced [17]. Fig. 3 shows the non-linearly varying stress distribution in x-direction σ_{xx} on the loading edges of stiffened panel loaded by a plastic bending. The strain distribution in x-direction ε_{xx} is assumed linear from the Mindlin–Reissner theory [36], expressed as:

$$\varepsilon_{xx}(y) = \frac{y - y_0}{h - y_0}\varepsilon_{xx}|_{y=h} \tag{1}$$

where y_0 represents the distance between the stiffener bottom edge and the neutral plane of stiffened panel which is dependent on σ_{xx} in the plastic region, and $\varepsilon_{xx}|_{y=h}$ represents the strain in x-direction where $y = h$ at the top surface of stiffener.

The Ramberg–Osgood equation is applied for the plastic behaviour of the material, given as [37]:

$$\varepsilon = \frac{\sigma}{E} + k_t \frac{\sigma_0}{E}\left(\frac{\sigma}{\sigma_0}\right)^{m_t} \tag{2}$$

where E represents Young's modulus, m_t, σ_0 and k_t represents the reciprocal of strain hardening exponent, offset yield stress and yield offset respectively.

The location of the neutral axis y_0 can be calculated by the equilibrium equation in x-direction, given as:

$$t_{st}\int_0^h \sigma_{xx}dy + b\int_{-t_{sk}}^0 \sigma_{xx}dy = \int_{-t_{sk}}^h F_X dy \tag{3}$$

where F_X is the normal force in x-direction per unit length. To solve the equilibrium equation in Eq. (3), the differential of y is supplanted by the differential of ε_{xx} and after integration by parts, Eq. (3) becomes [17]:

$$\begin{aligned} t_{st}\left[(h-y_0)\sigma_{xx}|_{y=h} + y_0\sigma_{xx}|_{y=0} - \frac{(h-y_0)}{\varepsilon_{xx}|_{y=h}}\int_{\sigma_{xx}|_{y=0}}^{\sigma_{xx}|_{y=h}} \varepsilon_{xx}d\sigma_{xx}\right] \\ +b\left[-y_0\sigma_{xx}|_{y=0} + (y_0 + t_{sk})\sigma_{xx}|_{y=-t_{sk}}\right. \\ \left. -\frac{(h-y_0)}{\varepsilon_{xx}|_{y=h}}\int_{\sigma_{xx}|_{y=-t_{sk}}}^{\sigma_{xx}|_{y=0}} \varepsilon_{xx}d\sigma_{xx}\right] = \int_{-t_{sk}}^h F_X dy \end{aligned} \tag{4}$$

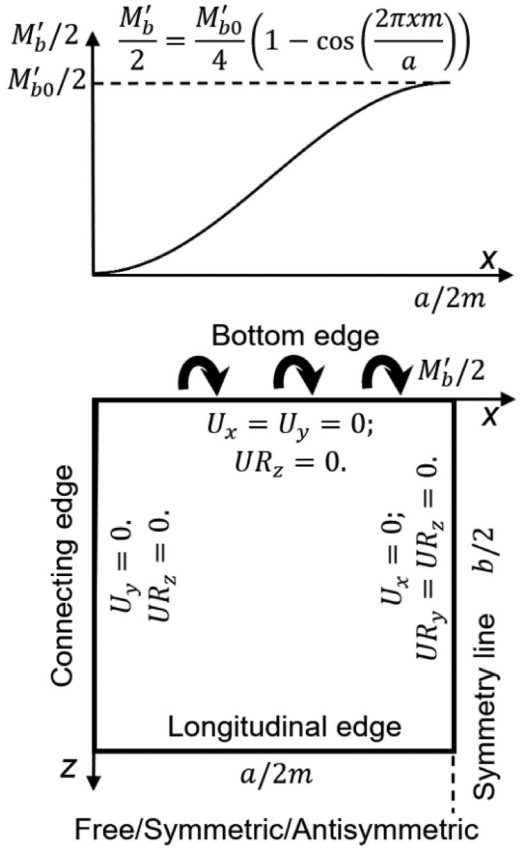


Fig. 4. FE model of skin applied to torsion along bottom edge.

When pure bending is the loading condition, the right side of Eq. (4) is zero due to the balanced resultant force F_X. For given stress at the top surface of stiffener $\sigma_{xx}|_{y=h}$, the corresponding y_0 is numerically obtained from Eq. (4) based on Newton's method.

2.4. Effective width

The previous studies [16,17] have found that the flexible skin effect on blade-stiffened panels in buckling analysis can be compensated by introducing the effective width b_{eff} in the boundary condition, which is determined as the width of a rigid panel with the same torsional stiffness as a flexible panel with width b. The effective widths b_{eff} for grid-stiffened panels with single stiffener and multiple stiffeners are calculated with FE simulations.

In the grid-stiffened panel, the deflection of the buckled longitudinal stiffener which has two constrained edges can be modelled as trigonometric functions based on Levy-type method, and the equivalent torsional moment on the bottom edge M_b' can be expressed as [38]:

$$M_b' = \frac{M_{b0}'}{2}\left(1 - \cos\left(\frac{2m\pi x}{a}\right)\right) \tag{5}$$

where M_{b0}' is the maximum torsion moment on the whole bottom edge, m represents the number of sinusoidal half-wave.

FE simulations with a commercial software Abaqus/Standard are conducted to study the flexible rotation response of the skin of grid-stiffened panels with single-stiffener and multi-stiffener cases subjected to the torsional moment along the bottom edge and the corresponding effective width b_{eff}. The FE model, which is a quarter of unit panel with one half-wave buckling mode using shell elements (S4R), as well as its boundary conditions are shown in Fig. 4. For single-stiffener cases, the boundary condition of the bottom edge is free and that with multi-stiffener cases is symmetric ($U_z = 0$ and $UR_x = UR_y = 0$) or anti-symmetric ($U_x = U_y = 0$ and $UR_z = 0$). The torsional moment $M_b'/2$ is applied to the model with a value of 10 (N m)/m [16]. The element size was set to $a/20$ [16]. Four groups of FE simulations with different geometric dimensions were conducted and the geometries with different length to width ratios a/b are listed in Table 1. The employed dimensions cover a wide range of a/b values from 0.125 to 3, in which a is constant in Groups 1 and 2, while b is constant in Groups 3 and 4.

Table 1
Skin dimensions for FE models (unit: mm).

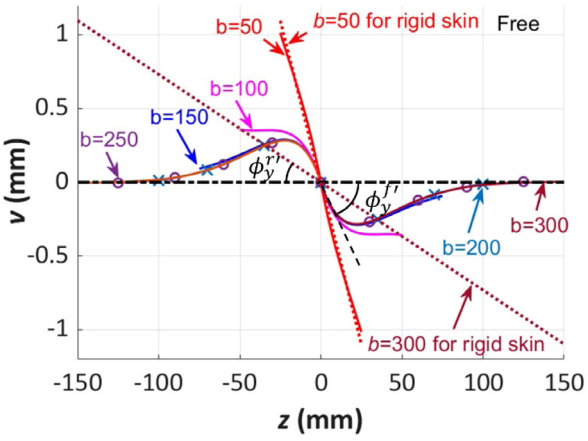
Group 1		Group 2		Group 3		Group 4	
a	b	a	b	a	b	a	b
50	12.5	100	50	800	100	532	200
50	37.5	100	100	160	100	229	200
50	62.5	100	150	90.0	100	146	200
50	87.5	100	200	60.0	100	107	200
50	112.5	100	250	47.0	100	84.2	200
50	137.5	100	300	38.0	100	69.6	200

Fig. 5(a)–(c) present the FE results of deformations in y-direction for flexible skins at the symmetric line for grid-stiffened panels respectively with free, symmetric and anti-symmetric boundary conditions on the longitudinal edge, where $\phi_y^{f'}$ and $\phi_y^{r'}$ are the angles of flexible skin and rigid skin. For the free boundary condition, when the width is small, the deformed flexible skin almost remains straight, and the rotation response of the flexible skin has a good agreement with the rigid skin. While the flexible skin becomes distorted and the rotation angle of flexible skin $\phi_y^{f'}$ becomes larger than that of rigid skin $\phi_y^{r'}$ with the increasing width. The results of the grid-stiffened panels with free boundary condition show a similar trend to those for the blade-stiffened panels in [16]. For the symmetric boundary conditions, the deformed flexible skin distorts with both ends parallel to the z axis, while the ends of the flexible skin are in contact with the z axis after torsion for the anti-symmetric boundary condition. For both two boundary conditions, the torsion stiffness of flexible skin is larger than that of rigid skin, especially for small width. The rotation behaviours of flexible skin with large width show similar results for the three boundary conditions.

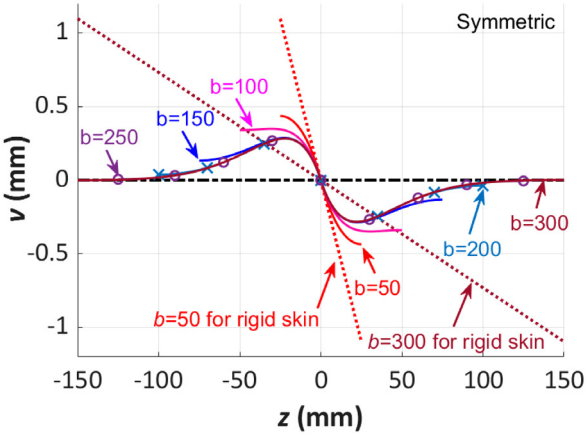
The effective width b_{eff} is captured from the FE simulations, and the expression is given as [16]:

$$b_{eff} \approx \frac{M_{b0}'\Delta x^2}{\left(\phi_y^{f'}\right)_{x=0} - 2\left(\phi_y^{f'}\right)_{x=\Delta x} + \left(\phi_y^{f'}\right)_{x=2\Delta x}} \frac{3}{Gt_{sk}^3} \tag{6}$$

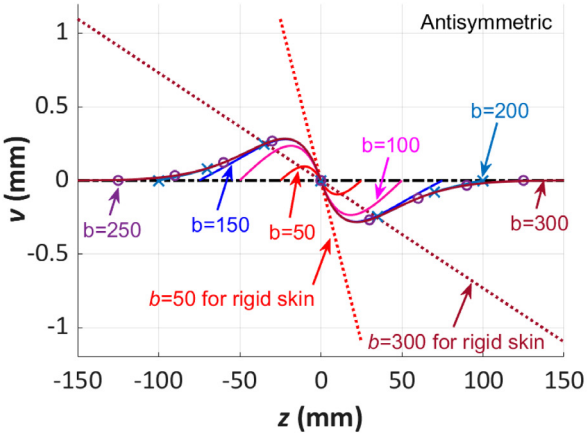
where G is shear modulus and Δx is the spatial increment of neighbouring nodes, which is the element size. Fig. 6 presents the FE simulated effective width for the grid-stiffened panels with single-stiffener and multi-stiffener cases. As shown in Fig. 6, all four groups of FE simulations with different skin aspect ratios b/a ranging from 0.125 to 3 (see Table 1 for dimensions) show the same trend. Therefore, the relations between mb_{eff}/a and mb/a with free, symmetric and anti-symmetric boundary conditions are independent of the geometric dimensions of grid-stiffened panels. For free boundary condition (single-stiffener cases), mb_{eff}/a increases linearly with the increasing mb/a initially and reaches a saturated state with further increasing mb/a values. For symmetric and anti-symmetric boundary conditions (multi-stiffener cases), mb_{eff}/a is relatively large at small mb/a due to the constraints on the longitudinal edges and high torsion stiffness for the flexible skin. When mb/a increases, mb_{eff}/a decreases when $mb/a < 0.5$, and then slightly increases to a stable state with a similar trend of the results with the free boundary condition. mb_{eff}/a with symmetric boundary condition is smaller than that with anti-symmetric boundary condition with small $mb/a < 1.37$, which indicates that the grid-stiffened panel will buckle in a U-shape for the skin region between two longitudinal stiffeners with small mb/a. The results of mb_{eff}/a with the three boundary conditions are the same for large widths ($mb/a > 1.37$), which reveals that the effect of multiple stiffeners can be neglected and either symmetric or



(a) Free boundary condition



(b) Symmetric boundary condition



(c) Antisymmetric boundary condition

Fig. 5. Deflection in y-direction of skin (v) for grid-stiffened panel with various widths b under the same torsion ($a = 100$ mm and $t_{sk} = 1$ mm). Solid lines are for flexible skin results and dotted lines are for rigid ones.

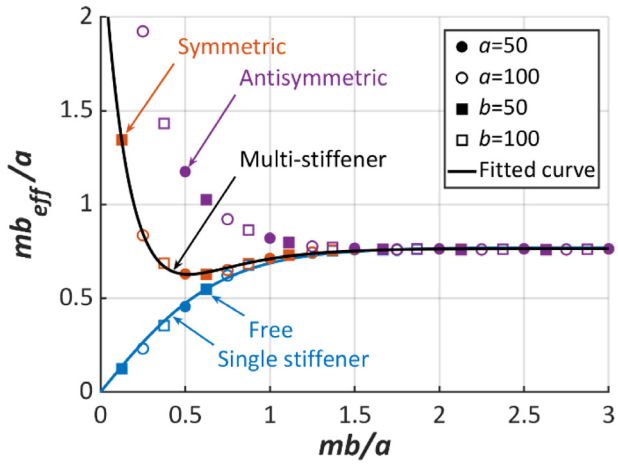


Fig. 6. Relationship between simulated effective width to length ratio mb_{eff}/a and actual ratio mb/a of grid-stiffened panels with single stiffener (Free) or multiple stiffeners (Symmetric or Antisymmetric boundary conditions).

antisymmetric boundary condition may be active (S- or M-shape for skin region will occur) when the width between longitudinal stiffeners is large ($mb/a > 1.37$).

The fitted curve for the multiple stiffeners case is obtained from the minimum values between the results with symmetric and antisymmetric boundary conditions. The fitted equations for the grid-stiffened panels with single stiffener and multiple stiffeners are given as:

$$b_{eff} = 0.7710\frac{a}{m}\tanh\left(\frac{1.432mb}{a}\right) \text{ (Single stiffener)} \tag{7}$$

$$b_{eff} = 2.556\frac{a}{m}e^{-\frac{6.092mb}{a}} + 0.7656\frac{a}{m}\tanh\left(\frac{1.595mb}{a}\right) \text{ (Multiple stiffeners)} \tag{8}$$

The accuracy of the effective width for grid-stiffened panels with single-stiffener or multi-stiffener cases is demonstrated later.

2.5. Boundary conditions

Assumed from the Mindlin–Reissner plate theory, the boundary conditions of grid-stiffened panel model are provided as [16,39]:

(a) EBI on the bottom edge ($y = 0$):

$$\begin{cases} w|_{y=0} = 0 \\ \phi_x|_{y=0} = 0 \\ \left(\dfrac{Gb_{eff}t_{sk}^3}{3}\dfrac{\partial^2\phi_y}{\partial x^2} + \dfrac{Et_{st}^3}{12}\left(\dfrac{\beta\partial\phi_x}{\partial x} + \dfrac{\gamma\partial\phi_y}{\partial y}\right)\right)_{y=0} = 0 \end{cases} \tag{9}$$

(b) Free on the top edge ($y = h$):

$$\begin{cases} M_{yy}|_{y=h} = 0 \\ M_{xy}|_{y=h} = 0 \\ Q_{yz}|_{y=h} = 0 \end{cases} \tag{10}$$

(c) EBI on the two loading edges ($x = 0, a$):

$$\begin{cases} w|_{x=0,a} = 0 \\ \phi_y|_{x=0,a} = 0 \\ \left(\dfrac{Gbt_{st}^3}{3}\dfrac{\partial^2\phi_x}{\partial y^2} + \dfrac{Et_{st}^3}{12}\left(\dfrac{\alpha\partial\phi_x}{\partial x} + \dfrac{\beta\partial\phi_y}{\partial y}\right)\right)_{x=0,a} = 0 \end{cases} \tag{11}$$

where

$$M_{yy} = \frac{Et_{st}^3}{12}\left(\frac{\beta\partial\phi_x}{\partial x} + \frac{\gamma\partial\phi_y}{\partial y}\right) \tag{12}$$

$$M_{xy} = \frac{Gt_{st}^3}{12}\left(\frac{\partial\phi_x}{\partial y} + \frac{\partial\phi_y}{\partial x}\right) \tag{13}$$

$$Q_{yz} = Gt_{st}\left(\phi_y + \frac{\partial w}{\partial y}\right) \tag{14}$$

M_{yy} and M_{xy} are the moment per unit length from σ_{yy} and σ_{xy}, and Q_{yz} is the resultant shearing force in yz-planes, α, β and γ are material constants depending on the plasticity theories.

3. Semi-analytical method

The semi-analytical method according to Mindlin–Reissner plate theory for acquiring buckling stress of stiffened panels loaded in bending was proposed in detail in [17]. In this study, the semi-analytical method is briefly introduced for completeness purposes. In the semi-analytical method, the equilibrium equation of the simplified model is solved to calculate the buckling stress by differential quadrature (DQ) method.

The rate form of the constitutive equation based on IT or DT of plasticity can be expressed as [40]:

$$\begin{bmatrix}\dot{\sigma}_{xx}\\ \dot{\sigma}_{yy}\\ \dot{\sigma}_{xy}\\ \dot{\sigma}_{yz}\\ \dot{\sigma}_{zx}\end{bmatrix} = \begin{bmatrix}\alpha E & \beta E & 0 & 0 & 0\\ \beta E & \gamma E & 0 & 0 & 0\\ 0 & 0 & 2G & 0 & 0\\ 0 & 0 & 0 & 2\kappa^2 G & 0\\ 0 & 0 & 0 & 0 & 2\kappa^2 G\end{bmatrix}\begin{bmatrix}\dot{\varepsilon}_{xx}\\ \dot{\varepsilon}_{yy}\\ \dot{\varepsilon}_{xy}\\ \dot{\varepsilon}_{yz}\\ \dot{\varepsilon}_{zx}\end{bmatrix} \tag{15}$$

where κ^2 is the Mindlin shear correction factor taken as 5/6 [41]. The expressions of α, β and γ based on different plasticity theories are given as:

(a) Based on IT of plasticity:

$$\alpha = \frac{1}{\rho}\left[1 + 3\frac{E_t}{E}\right],\quad \beta = \frac{1}{\rho}\left[2 - 2(1-2\nu)\frac{E_t}{E}\right],\quad \gamma = \frac{4}{\rho},$$
$$G = \frac{E}{2+2\nu},\quad \rho = (5-4\nu) - (1-2\nu)^2\frac{E_t}{E} \tag{16}$$

(b) Based on DT of plasticity:

$$\alpha = \frac{1}{\rho}[1 + 3\frac{E_t}{E_s}],\quad \beta = \frac{1}{\rho}\left[2 - 2(1-2\nu)\frac{E_t}{E}\right],\quad \gamma = \frac{4}{\rho},$$
$$G = \frac{E}{2+2\nu+3\left(\frac{E}{E_s}-1\right)},\quad \rho = \frac{3E}{E_s} + (1-2\nu)\left[2 - (1-2\nu)\frac{E_t}{E}\right] \tag{17}$$

where ν is Poisson's ratio, E_t is the tangent modulus of the material and E_s is the secant modulus, which can be calculated from Eq. (2):

$$\frac{E}{E_t} = 1 + m_t k_t\left(\frac{\sigma}{\sigma_0}\right)^{m_t - 1} \tag{18}$$

$$\frac{E}{E_s} = 1 + k_t\left(\frac{\sigma}{\sigma_0}\right)^{m_t - 1} \tag{19}$$

The rate form of the equilibrium equations in the elastic–plastic region can be expressed by σ_{xx} [17]:

$$\begin{bmatrix} \kappa^2 G\frac{\partial}{\partial x} & \kappa^2 G\frac{\partial}{\partial y} & \kappa^2 G\left(\frac{\partial^2}{\partial x^2} + \frac{\partial^2}{\partial y^2}\right)\\ \frac{\alpha E t_{st}^3}{12}\frac{\partial^2}{\partial x^2} + \frac{G t_{st}^3}{12}\frac{\partial^2}{\partial y^2} - \kappa^2 G t_{st} & \frac{\partial^2}{\partial x\partial y}\left(\frac{\beta E t_{st}^3}{12} + \frac{G t_{st}^3}{12}\right) & -\kappa^2 G t_{st}\frac{\partial}{\partial x}\\ \frac{\partial^2}{\partial x\partial y}\left(\frac{\beta E t_{st}^3}{12} + \frac{G t_{st}^3}{12}\right) & \frac{\gamma E t_{st}^3}{12}\frac{\partial^2}{\partial y^2} + \frac{G t_{st}^3}{12}\frac{\partial^2}{\partial x^2} - \kappa^2 G t_{st} & -\kappa^2 G t_{st}\frac{\partial}{\partial y}\end{bmatrix}$$
$$\cdot\begin{bmatrix}\phi_x\\ \phi_y\\ \dot{w}\end{bmatrix} = \sigma_{xx}\begin{bmatrix}\frac{\partial^2}{\partial x^2} & 0 & 0\\ 0 & 0 & 0\\ 0 & 0 & 0\end{bmatrix}\begin{bmatrix}\phi_x\\ \phi_y\\ \dot{w}\end{bmatrix} \tag{20}$$

where $\dot{w}$ stands for the velocity in z-direction, $\dot{\phi}_x$ and $\dot{\phi}_y$ are the rate form of rotations of longitudinal stiffener about y-axis and x-axis, respectively.

DQ method is applied to solve the equilibrium equations in Eq. (20) to acquire buckling stresses of grid-stiffened panels loaded in bending. In DQ method, the simplified model is discretised into $N \times N$ grid points and equilibrium equations are generated on each grid point. The derivatives at each point can be approximately calculated by the value in the same row or column.

The equilibrium equations at inner points in Eq. (20) and boundary condition at four-edge points in Eqs. (9)–(11) are merged into a generalised eigenvalue equation to calculate the buckling stress σ_b as:

$$[A]\left[\dot{w}, \dot{\phi}_x, \dot{\phi}_y\right]^T = \sigma_b[B]\left[\dot{w}, \dot{\phi}_x, \dot{\phi}_y\right]^T \tag{21}$$

where $[A]$ is the matrix of the left-hand side of the generalised eigenvalue equation for all grid points, and $[B]$ is the matrix of σ_b. In the generalised eigenvalue equation (Eq. (21)), $\left[\dot{w}, \dot{\phi}_x, \dot{\phi}_y\right]^T$ and σ_b are the generalised eigenvector and eigenvalue of $[A]$ and $[B]$, which can be obtained by solving Eq. (21).

The non-dimensional critical buckling coefficient k_{cr} is calculated to study the effects of geometric dimensions, multiple stiffeners and temperature on buckling responses of grid-stiffened panels, and the expression is given as [42]:

$$k_{cr} = \frac{12(1-\nu^2)\sigma_b h^2}{E\pi^2 t_{st}^2} \tag{22}$$

The iterative method has been used in the semi-analytical method due to changing material constants in the plastic region, and the flow chart of the semi-analytical method is presented in Fig. 7. The iterative method has two loops which combine the outer loop for the calculation of critical buckling stress and the inner loop for ensuring the consistency between the buckling mode and the effective width considering the effect of flexible skin on buckling of stiffened panels. To ensure the convergence of k_{cr} with four significant figures, N is set as 29 for $t_{st} < 1$ mm and 21 for $t_{st} \le 1$ mm [17].

4. Finite element method

The buckling FE model for grid-stiffened panel with single stiffener [10] and a new model with multiple stiffeners were applied with the commercial software Abaqus/Standard to verify the effectiveness of the simplified model of grid-stiffened panel in the semi-analytical method. It has been reported that buckling mainly occurs in the loading or heating stages [10], thus the buckling analysis of grid-stiffened panel loaded by four point bending was conducted at room and ageing temperatures by non-linear FE simulations. The new FE model of grid-stiffened panels with multiple stiffeners and the corresponding boundary conditions in four-point bending are shown in Fig. 8. The single-stiffener model was modelled by the grid-stiffened panel with two transverse stiffeners and single longitudinal stiffener, and the multi-stiffener model was modelled by the grid-stiffened panel with six longitudinal stiffeners to study the influence of multiple stiffeners. Both grid-stiffened panels were modelled using shell elements (S4R). In the models, upper and bottom rollers were used to apply bending moment on the grid-stiffened panel, with radii of 10 and 25 mm. The elements used for the upper and bottom rollers were discrete rigid shell elements (R3D4). A mesh size of 2 mm was selected for both the grid-stiffened panels and the rollers according to convergence tests to achieve a difference within 0.5%. The distances between two upper rollers and two bottom rollers were 60 mm and 260 mm, respectively. The boundary conditions of both models are presented in Fig. 8, in which the middle line ($x = 0$) of the skin along z-direction is fixed in x-direction ($U_x = 0$) and two middle lines ($z = 0$) at two ends of the model along y-direction are fixed in z-direction ($U_z = 0$). The bottom rollers were fully constrained, and the upper rollers could only translate in y-direction. The employed friction coefficient between the grid-stiffened panel and the rollers was 0.1 [43].

There are three stages in the FE simulation for buckling analysis, including gravity (create initial contacts between bottom rollers and stiffened panel), pre-loading (translate upper rollers in y-direction by −0.1 mm to create initial contacts between upper rollers and stiffened

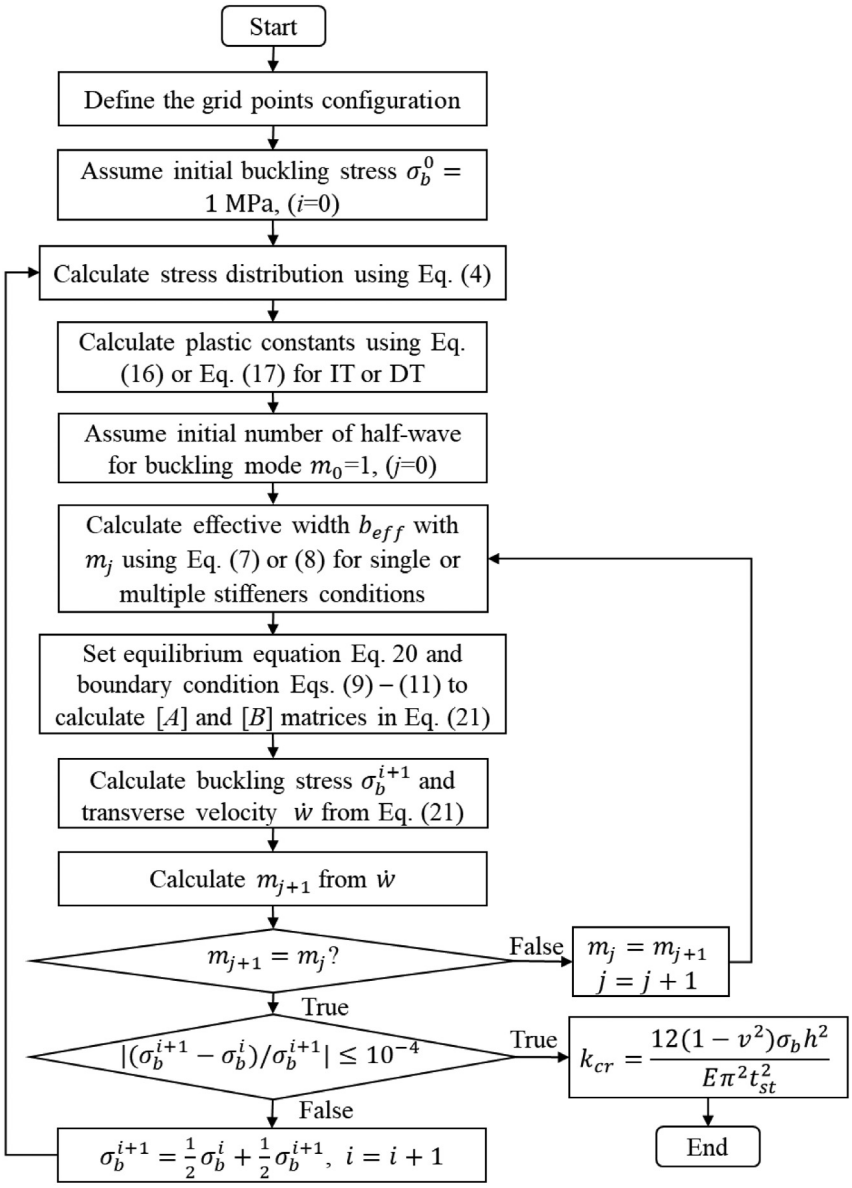


Fig. 7. Flow chart for elastic–plastic buckling analysis using semi-analytical method.

panel), and loading (apply load on upper rollers to bend stiffened panel).

Two FE methods, the eigenvalue FE method and non-linear FE method according to Riks method, were applied successively to analyse the buckling response of grid-stiffened panels at room and ageing temperatures using different material properties at two temperatures. Initial imperfections, first-order buckling mode with an amplitude of 0.2% stiffener thickness, were obtained from eigenvalue FE method [10]. Then, non-linear FE simulations with the initial geometric imperfections were carried out to calculate the buckling stress of grid-stiffened panels.

Fig. 9 presents the buckling mode of grid-stiffened panels with multiple stiffeners loaded by bending with normalised deflection (Normalised deflection = Deflection/Maximum deflection). Buckling occurs on the longitudinal stiffeners for grid-stiffened panels with multi-stiffener, which shows similar buckling behaviour to the experimental results in [10]. For the multi-stiffener cases, the deflection of each adjacent longitudinal stiffener was symmetrical with symmetric boundary condition between each unit cell. The CPU times spent for the buckling analysis of stiffened panels were about 11 and 135 min respectively for eigenvalue FE method and non-linear FE method with Intel Core i7-6700 at 3.4 GHz with 16.0 GB of RAM, and thus, the total CPU time was around 146 min; while the semi-analytical method took only 2 min to solve the buckling problem of the same stiffened panel using the same computer, indicating a time saving of 98.6% by the semi-analytical method.

5. Results and discussions

5.1. Effectiveness of semi-analytical method

The semi-analytical method was applied to predict the buckling strain ε_{cr} of grid-stiffened panel with single stiffener subjected to

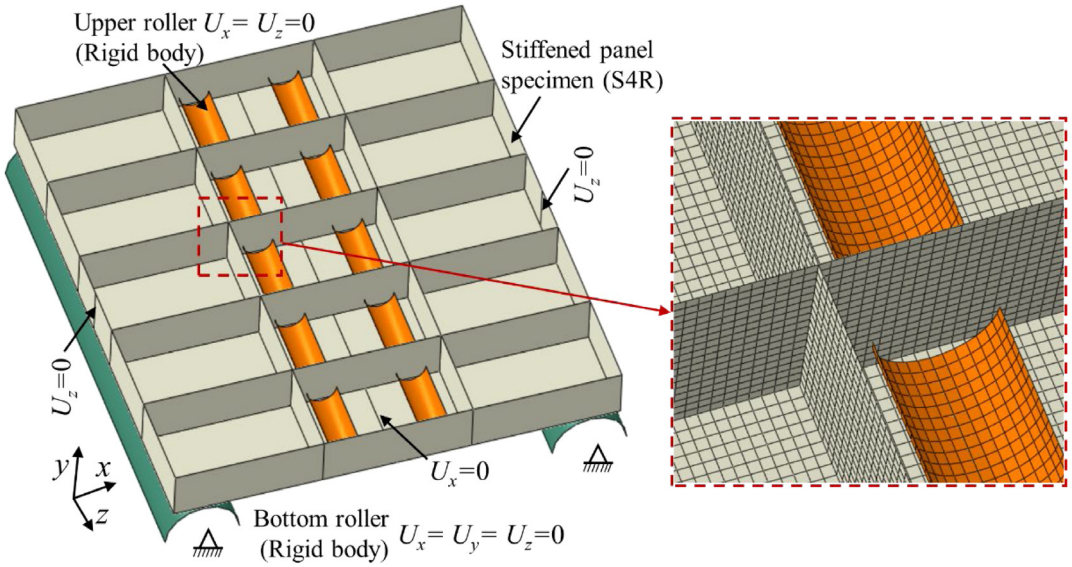


Fig. 8. Buckling FE model of panel with multiple grid stiffeners.

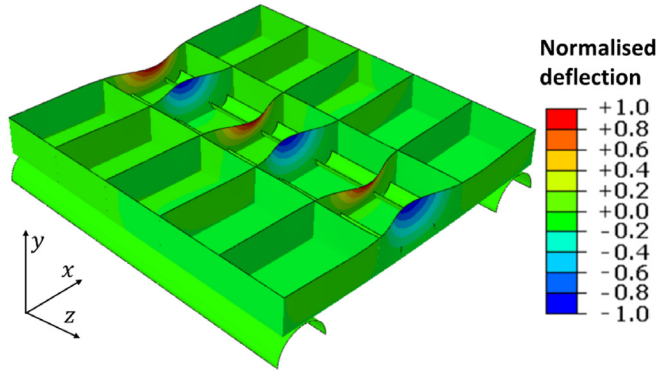


Fig. 9. Buckling mode of panels with multiple grid stiffeners from non-linear FE method.

bending and compared with the experimental results in [10] to verify its effectiveness. The Ramberg–Osgood form of the basic material properties of AA7050-T7451 at room temperature was used for the semi-analytical method, as $E = 68$ GPa, $\sigma_0 = 489$ MPa, $\nu = 0.33$, $k_t = 0.439$ and $m_t = 41.5$ which is fitted from the stress–strain curve in [10], for demonstration in this study. Fig. 10(a) presents the relation between stiffener thickness t_{st} and the buckling strains ε_{cr} of grid-stiffened panels from experimental results and the corresponding FE results and the semi-analytical results based on IT and DT, while Fig. 10(b) shows the results with different stiffener heights h. The FE results agree well with the experimental results. For the semi-analytical results of buckling strain, the magnitude of the results based on DT are generally smaller than those based on IT. The magnitude of critical buckling strain results based on DT increase almost linearly with increasing t_{st} and decreasing h, while those based on IT increase at an increasing rate with increasing t_{st} and decreasing h. For both IT and DT results, buckling mode change occurs when entering the plastic region with increasing t_{st} and decreasing h. Compared with the experimental results, the semi-analytical results based on IT present good agreement, which reveals that IT is the appropriate plasticity theory to resolve buckling issues of grid-stiffened panels loaded by plastic bending.

From the comparison between experimental results and semi-analytical results above, the semi-analytical method based on IT and non-linear FE method can predict buckling stress with high accuracy while the proposed semi-analytical method based on DT provides lower predictions. Based on the developed semi-analytical method and the non-linear FE method, the effects of geometric dimensions, multiple stiffeners and temperature on buckling behaviours of grid-stiffened panels will be investigated in the following sections.

5.2. Effects of geometric dimensions

This section will focus on the effects of geometric dimensions on the buckling response of grid-stiffened panels with single stiffener, using the semi-analytical method and non-linear FE method. The buckling response of blade-stiffened panels with the corresponding geometric parameters was also investigated using the method in [17] for comparison.

(a) Thickness to height ratio and plasticity theory

Fig. 11(a) presents the relation between critical buckling coefficient k_{cr} of the grid-stiffened panels and thickness to height ratios t_{st}/h from FE method and the semi-analytical method with IT and DT in comparison with that of the blade-stiffened panels, which covers elastic and plastic buckling responses. The effective width b_{eff} was used in the semi-analytical method to consider the flexible skin effect. For both types of stiffened panels, k_{cr} based on DT is close to that on IT. When t_{st}/h is smaller than 0.07, buckling occurs in the elastic region and elastic buckling coefficient k_{cr} slightly declines linearly with increasing t_{st}/h because of shear effects through the thickness of stiffener. The elastic results of the grid-stiffened panels are 14% larger than that of blade-stiffened panels. When t_{st}/h further increases, plastic buckling occurs and k_{cr} decreases faster for both types of stiffened panels. For grid-stiffened panels, the transition points of elastic–plastic buckling results happen earlier than those for blade-stiffened panels. The decreasing rate of k_{cr} for grid-stiffened panels in plastic region is slightly larger than that for blade-stiffened panels, which leads to the continuously decreasing difference of k_{cr} between the two types of stiffened panels when t_{st}/h increases. When $t_{st}/h > 0.08$, results from all methods (DT, IT, blade, grid, or FE) are almost the same.

Fig. 11(b) shows the results of the normalised buckling strain $E\varepsilon_{cr}/\sigma_0$ of stiffened panels with different t_{st}^2/h^2 from the FE method and

the semi-analytical method. The magnitude of $E\varepsilon_{cr}/\sigma_0$ of grid-stiffened panels is larger than that of blade-stiffened panels for both elastic and plastic results. This indicates that transverse stiffeners enhance buckling resistance of grid-stiffened panels. For both stiffened panels, the normalised buckling compressive strain $E\varepsilon_{cr}/\sigma_0$ increases linearly with increasing t_{st}^2/h^2 in the elastic region and the results according to IT and DT are the same. The results according to IT and DT start to separate when $E\varepsilon_{cr}/\sigma_0 = 1$ and the system enters the plastic buckling region. In plastic region, the compressive strain results based on DT increase less quickly with increasing t_{st}^2/h^2 compared with the elastic results, while those based on IT increase more quickly, showing that the differences between the results from IT and DT increase with increasing t_{st}^2/h^2. This is due to smaller material constants α, β, γ and G based on DT in the plasticity than those based on IT [17]. For the results based on IT, there is a small change for the rate of k_{cr} for both types of stiffened panels at t_{st}^2/h^2 of 0.0073 because of the change of buckling mode. This phenomenon is consistent with the experimental results [10]. It can be seen from Fig. 11 that the results from the semi-analytical methods based on IT agree well with non-linear FE results for grid and blade-stiffened panels in elastic and plastic regions. The difference between the results with the two methods is within 4.4%. Therefore, IT predicts buckling results with good accuracy and DT provides a lower prediction.

To study the influences of other geometric parameters on buckling response in elastic and plastic regions, t_{st}/h was selected as 0.04 and 0.09 for the following cases. Only IT was applied in the following calculations since IT provides more accurate predictions.

(b) Width to height ratio and effective width

The semi-analytical results and FE results of k_{cr} with stiffened panel width b and effective width b_{eff} considering the flexible skin effect versus width to height ratio b/h are presented in Fig. 12. Fig. 12(b) shows the plastic results with $t_{st}/h = 0.09$ in detail. For elastic and plastic results of the grid and blade-stiffened panels, difference between the semi-analytical results with b and non-linear FE results becomes larger with growth of b/h, while the results with b_{eff} achieve a higher accuracy. When $t_{st}/h = 0.04$, elastic results of k_{cr} rises with a small b/h and then keeps static as b/h increases. When $t_{st}/h = 0.09$, plastic results of k_{cr} increases at first and then declines lightly with growth of b/h, in which the buckling mode changes as shown in Fig. 13(b). This is because that the torsional stiffness of skin enhances with growth of b/h, leading to the increase of k_{cr} at the initial stage. When b continues to increase, k_{cr} becomes static since the torsional stiffness of flexible skins tends to remain stable with increasing b, as shown in Fig. 5(a). The slight drop of neutral plate causes very small reduction of k_{cr} with further rise of b/h. k_{cr} of grid-stiffened panel is larger than that of blade-stiffened panel. As shown in Fig. 13(b), the effect of b on k_{cr} in the plastic region is generally very small. The higher accuracy of the semi-analytical method with b_{eff} is validated by the non-linear FE results and thus, b_{eff} is applied to the semi-analytical method in the following calculations.

(c) Length to height ratio

The influence of the length to height ratio a/h on k_{cr} of grid-stiffened panels is presented in Fig. 13. When $t_{st}/h = 0.04$, a relatively high elastic result of k_{cr} is observed when $a/h < 2$, and k_{cr} declines dramatically with increasing a/h until reaching a static region. As shown in Fig. 13, k_{cr} repeated decreasing–increasing cycles in the stable region at a much smaller scale, where the buckling modes vary from one to higher-order half-wave for each cycle. At a small a/h, k_{cr} of grid-stiffened panels is almost 2 times that of blade-stiffened panels, while the difference of k_{cr} between two types of stiffened panels reduces with growth of a/h because the effect of EBI boundary condition decreases. The difference of k_{cr} decreases to less than 2% when a/h increases above 5. When $t_{st}/h = 0.09$, k_{cr} decreases slowly and then remains stable with increasing a/h. k_{cr} of grid-stiffened panels is slightly larger than that of blade-stiffened panels at small a/h value and those two become the same after a/h increases. The results from semi-analytical method based on IT presents a good agreement with non-linear FE simulations for both types of stiffened panels.

(d) Thickness ratio

The relationship between thickness ratio t_{sk}/t_{st} and k_{cr} of grid and blade-stiffened panels is shown in Fig. 14. When t_{sk}/t_{st} increases, the skin rotational constraint will increase and the distance between the bottom edge and the neutral plane of stiffened panels y_0 will decrease. Therefore, k_{cr} first increases as t_{sk}/t_{st} increases, when $t_{st}/h = 0.04$. It then remains stable with slight increase since buckling modes turn from one to two half-waves (indicated in Fig. 14). The difference between k_{cr} for both types of stiffened panels keeps stable as t_{sk}/t_{st} increases. When $t_{st}/h = 0.09$, there is a small increase of k_{cr} of blade-stiffened panels at small $t_{sk}/t_{st,}$ while k_{cr} of grid-stiffened panels remains stable at all t_{sk}/t_{st}. Again, k_{cr} based on IT using b_{eff} presents a good agreement with non-linear FE results for both types of stiffened panels.

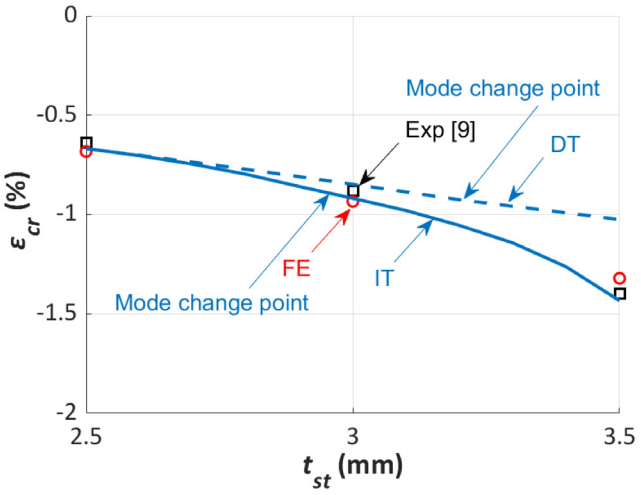
5.3. Effect of multiple stiffeners

The effect of multiple stiffeners on k_{cr} of grid-stiffened panel was investigated using the semi-analytical method with the effective width b_{eff} of multi-stiffener cases and non-linear FE simulations. The results of grid-stiffened panel with single stiffener and multiple stiffeners are shown in Fig. 15. k_{cr} with multiple stiffeners cases remains static with the selected width to height ratio b/h for both elastic and plastic results. Compared with single stiffener cases, grid-stiffened panels with multiple stiffeners have higher k_{cr} at small b/h. The difference between k_{cr} with multiple stiffeners and single stiffener cases diminishes with increasing b/h, which reveals that the effect of multiple stiffeners can be neglected with a relatively large b/h. The semi-analytical results of grid-stiffened panels with multiples stiffeners and the FE results have achieved a good agreement.

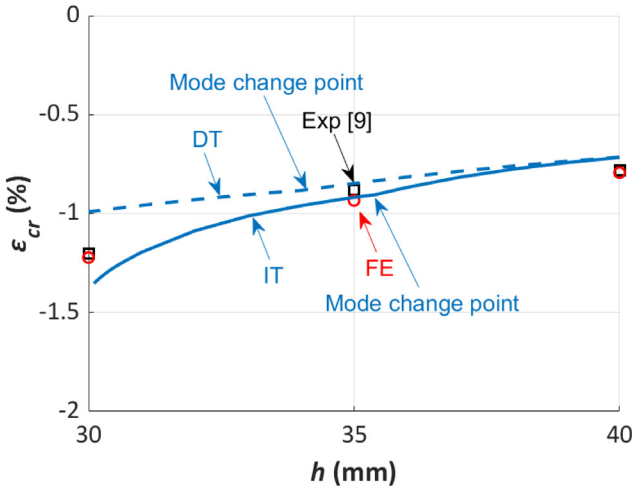
5.4. Effect of temperature

The buckling response of grid-stiffened panel loaded in bending at the ageing temperature is investigated by the semi-analytical method and non-linear FE simulations using AA7050-T7451. The basic material properties of AA7050-T7451 at the ageing temperature of 160 °C were determined from the tensile test results in [10], with the following values for parameters in Eq. (2) as $E = 68$ GPa, $\sigma_0 = 386$ MPa, $k_t = 0.335$ and $m_t = 118$. Fig. 16(a) shows k_{cr} of grid-stiffened panels versus the thicknesses to height ratio t_{st}/h at room and ageing temperatures. In the elastic region, k_{cr} at the two temperatures are the same and decreases slightly with increase of t_{st}/h. Rapid decrease of k_{cr} in the plastic region can be observed at both temperatures. The decrease of k_{cr} at the ageing temperature occurs at lower t_{st}/h value compared with room temperature condition due to lower yield stress of the material at the ageing temperature. In plastic region, lower k_{cr} at the ageing temperature compared with room temperature, indicates that the buckling stress decreases in the heating stage of CAF when loading enters plastic region. The results from the semi-analytical method based on IT present good agreement with the results of FE simulations at the two temperatures.

To compare the buckling results at the two temperatures, Fig. 16(b) presents the effect of temperature on the critical buckling strain ε_{cr} with different t_{st}^2/h^2 from the semi-analytical method and non-linear FE simulations. The results at the ageing temperature from the semi-analytical method have achieved a good agreement with non-linear FE results. When $t_{st}^2/h^2 < 4 \times 10^{-3}$, the elastic buckling at the two temperatures occurs and the results are the same. When $4 \times 10^{-3} < t_{st}^2/h^2 < 6 \times 10^{-3}$, the magnitude of ε_{cr} at the ageing temperature is lower compared with room temperature and the stiffened panel at the ageing temperature enters plastic region earlier than that at room temperature. When t_{st}^2/h^2 continues to increase, the magnitude of ε_{cr} at the ageing temperature becomes larger than that at room temperature, due to lower strain hardening behaviour at the ageing temperature.



(a) Results with different stiffener thicknesses t_{st} (h = 35 mm).

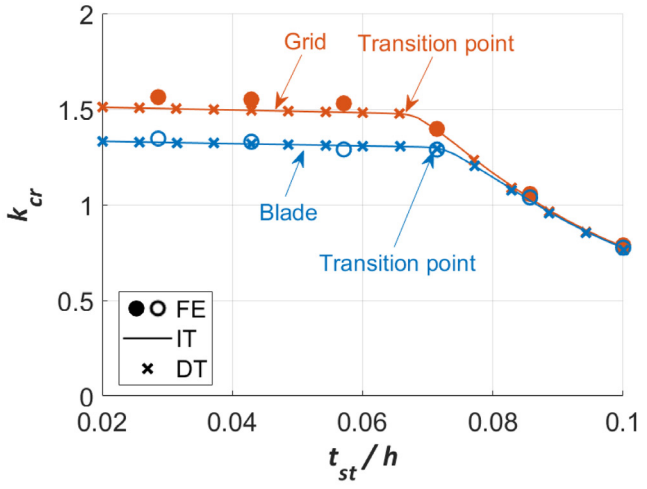


(b) Results with different stiffener heights h (t_{st} = 3 mm).

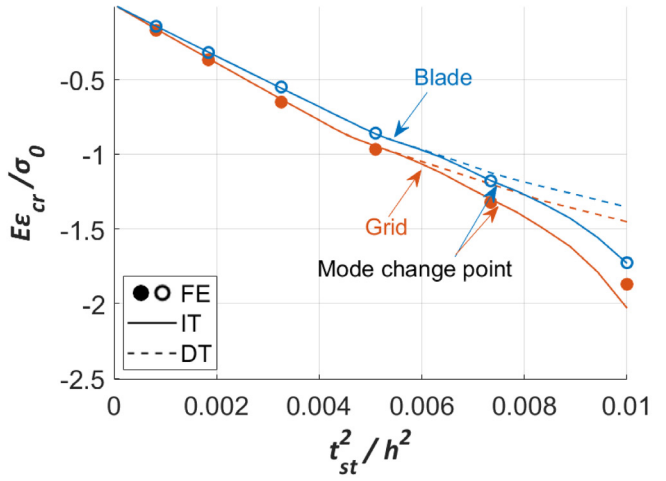
Fig. 10. Comparison of buckling strain ε_{cr} of stiffened panel experiments among the experimental (square symbols) [10], non-linear FE (circular symbols) and semi-analytical results (DT with dish line and IT with solid line) (a = 100 mm, b = 65 mm and t_{sk}/t_{st} = 1).

The buckling strain prediction from the semi-analytical method reveals that, for the stiffened panel with t_{st}^2/h^2 in the region between 4×10^{-3} and 6×10^{-3}, buckling may take place during the heating stage even though no buckling is found in the loading stage. If $t_{st}^2/h^2 > 6 \times 10^{-3}$, the formability of stiffened panel will increase in the heating stage, and buckling will not take place in the heating process. When $t_{st}^2/h^2 > 8 \times 10^{-3}$, a sharp increase in the buckling strain can be observed at the ageing temperature, which leads to violation of the small deformation assumption in the Mindlin–Reissner plate theory. This is caused by the very low strain hardening (i.e. large m_t) of the material used in this study at the ageing temperature. Similar phenomena have been reported in other publications for plates under compression [39,44].

In this section, the effectiveness of the semi-analytical method has been demonstrated by comparing with the published experimental results in [10]. Based on the semi-analytical method, the effects of geometric dimensions, multiple stiffeners and temperature have been investigated. The buckling coefficients of grid-stiffened panels are larger than those of blade-stiffened panels, which indicates that the transverse stiffener can enhance the buckling resistance of grid-stiffened panels. The difference of buckling strains between grid- and blade-stiffened panels increases with the increase of stiffener thickness to stiffener height ratio t_{st}/h or the decrease of length to height ratio a/h. However, the effect of transverse stiffener leading to the rise of buckling coefficient k_{cr} is insensitive to thickness ratio t_{sk}/t_{st} and width to height ratio b/h. The stiffened panels with multiple stiffeners have a slightly higher buckling coefficient k_{cr} with small b/h, the effect of multiple stiffeners diminishes with increasing b/h. The buckling strain at the ageing temperature is the same as that at room temperature when $t_{st}/h < 4 \times 10^{-3}$, in which the loading is in the elastic region, while the results at the ageing temperature will first become smaller than the room temperature results and then become larger with further increase of t_{st}/h. In addition, the type of stiffener for the proposed method in this study is blade stiffener, which can be extended to complex stiffeners, such as T-, J-, I-, Z- stiffener, by modifying the free boundary conditions

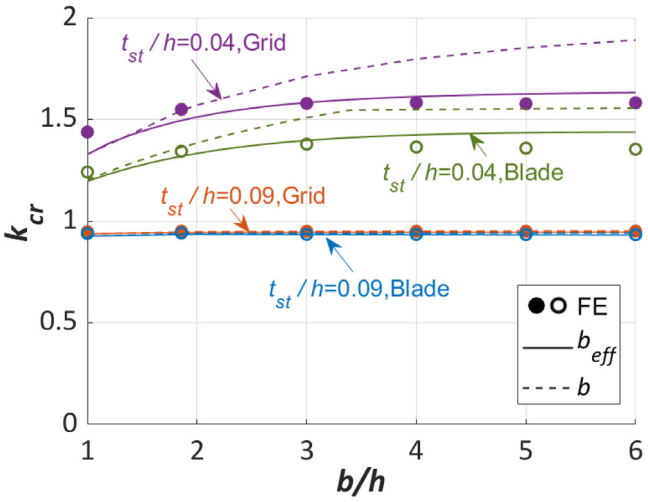


(a) Critical buckling coefficient k_{cr}

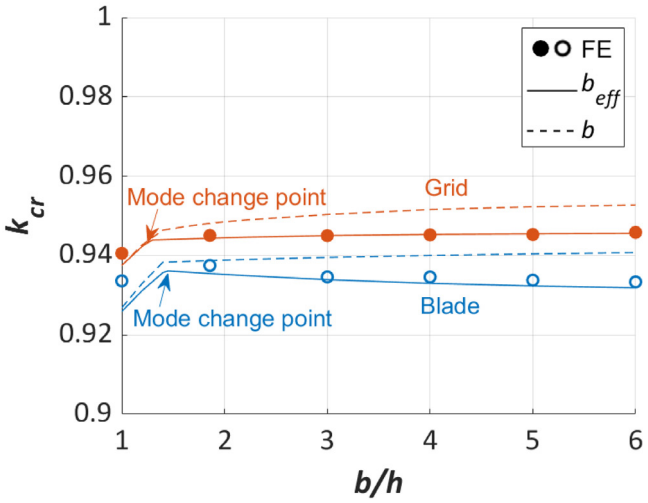


(b) Normalised critical buckling strain $E\varepsilon_{cr}/\sigma_0$

Fig. 11. Comparison between results of grid-stiffened panels and blade-stiffened panels from non-linear FE simulations and semi-analytical method with IT and DT with b_{eff} ($a/h = 2.9$, $b/h = 1.9$ and $t_{sk}/tst = 1.0$).



(a) Elastic and plastic regions



(b) Plastic region ($t_{st}/h = 0.09$)

Fig. 12. Comparison between k_{cr} of grid-stiffened panels and blade-stiffened panels from semi-analytical method based on IT (solid lines for b_{eff} and dashes lines for b) and non-linear FE method (symbols) as a function of b/h ($a/h = 2.9$ and $t_{sk}/t_{st} = 1.0$). (b) is an enlarged part of (a), showing more detail in the plastic region.

on the top edges of the simplified model to elastically built-in condition relating to the type and geometry of stiffener. Currently, the proposed method is not suitable for the buckling analysis of the stiffened panels with complex grids (such as triangle grid and isogrid) under bending. Further work is required to solve the buckling problem of complex grid panels analytically.

6. Conclusions

Simplified models of grid-stiffened panels with single stiffener or multiple stiffeners under CAF in the semi-analytical method have been proposed. Incremental and deformation theories of plasticity have been applied to the semi-analytical method. The effectiveness of semi-analytical method with IT has been validated through the buckling experiments and non-linear FE method. Based on the developed methods, the effects of geometric dimensions, transverse stiffener, multiple stiffeners and temperature on buckling response of grid-stiffened panels have been studied. The following conclusions can be drawn:

- The buckling strain results from the semi-analytical method with IT achieve good agreement with experimental and FE results within the stiffener thickness to height ratio range studied ($t_{st}/h \leq 0.1$), while the results with DT consistently provide a lower buckling strain prediction in the plastic region.
- Effective width b_{eff}, introduced for the semi-analytical method for grid-stiffened panels to consider the effects of flexible skin and multiple stiffeners, is independent of the stiffened panel geometric dimensions and an efficient simplification of the complex geometry. It promotes the accuracy of the predictions for buckling stress and decreases the maximum difference between FE results and semi-analytical results from 19.5% to 6.2%.
- In elastic region, the critical buckling coefficient k_{cr} for grid-stiffened panels decreases from around 4 to 1.3 with the increase

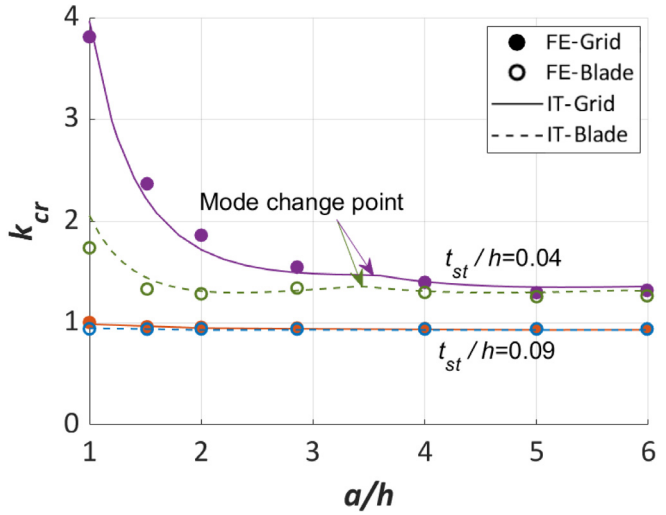


Fig. 13. Comparison between k_{cr} of grid-stiffened panels and blade-stiffened panels from semi-analytical method based on IT with b_{eff} (solid lines) and non-linear FE method (symbols) versus a/h (b/h = 1.9 and t_{sk}/t_{st} = 1.0).

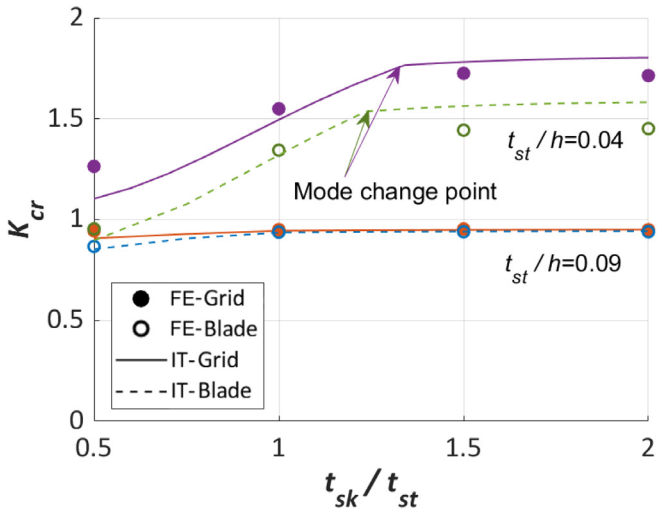


Fig. 14. Comparison between k_{cr} of grid-stiffened panels and blade-stiffened panels from semi-analytical method based on IT with b_{eff} (solid lines) and non-linear FE method (symbols) versus t_{sk}/t_{st} (a/h = 2.9 and b/h = 1.9).

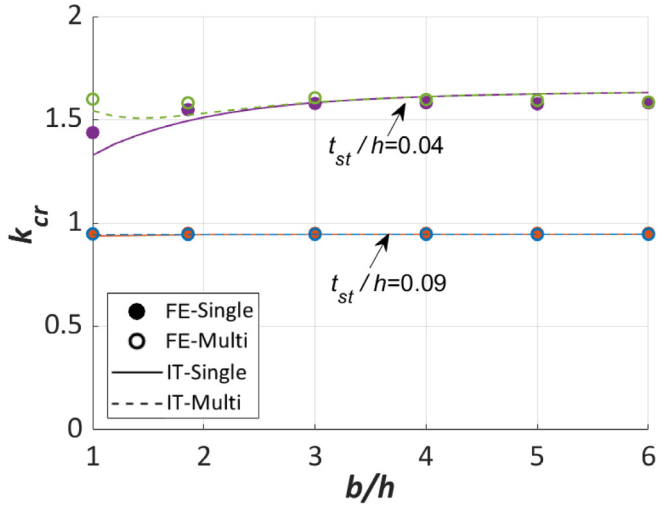
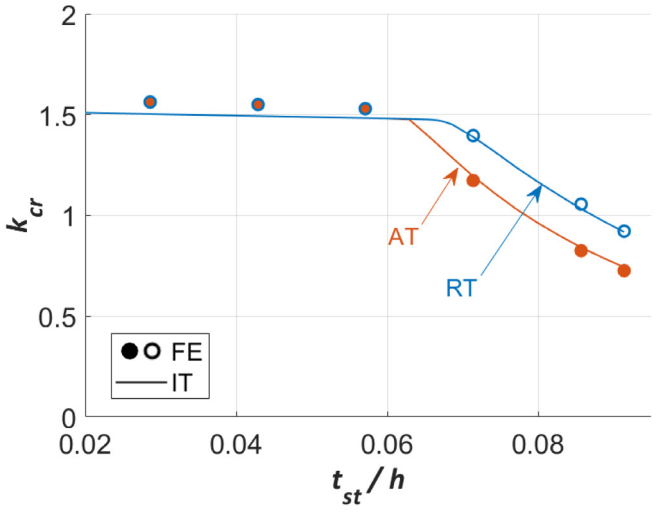
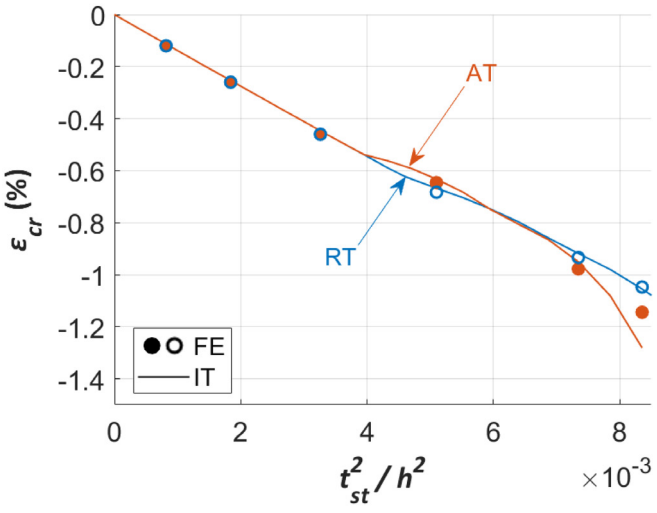


Fig. 15. Comparison between k_{cr} of grid-stiffened panels with single stiffener or multiple stiffeners from semi-analytical method based on IT with b_{eff} (solid lines) and non-linear FE method (symbols) versus b/h (a/h = 2.9 and t_{sk}/t_{st} = 1.0).



(a) Critical buckling coefficient k_{cr}



(b) Critical buckling strain ε_{cr}

Fig. 16. Buckling results from semi-analytical method based on IT with b_{eff} and FE method at room temperature (RT) and ageing temperature (AT) (a/h = 2.9, b/h = 1.9 and t_{sk}/t_{st} = 1.0).

of length to height ratio from 1 to 6. With increasing width to height ratio from 1 to 6, k_{cr} initially increases by about 20% then remains constant. Increasing thickness ratio from 0.5 to 2 results in the increase of k_{cr} by around 70%. In plastic region, k_{cr} decreases by 49% with increasing t_{st}/h from 0.02 to 0.1, while almost stays constant with increasing a/h, b/h and t_{sk}/t_{st}.

- The transverse stiffener enhances the buckling coefficient by around 14%, and the effect decreases with the increase of the length to height ratio. Multiple stiffeners increase the buckling coefficient by around 11% only when the width to height ratio is very small, while the effect of multiple stiffeners is negligible when b/h is larger than 2.5.
- In elastic–plastic region, the buckling strain at the ageing temperature is lower than room temperature condition due to lower yield

strength at the ageing temperature. However, in plastic region, opposite phenomenon occurs due to lower strain hardening at the ageing temperature. This indicates that during CAF, buckling may occur in the heating stage on the panel with no buckling in the loading stage when $4 \times 10^{-3} < t_{st}^2/h^2 < 6 \times 10^{-3}$, while buckling will not occur in the heating stage when $t_{st}^2/h^2 \geq 6 \times 10^{-3}$.

CRediT authorship contribution statement

Wenbin Zhou: Writing – original draft, Methodology, Investigation. **Zhusheng Shi:** Writing – review & editing, Supervision, Funding acquisition, Conceptualization. **Jianguo Lin:** Writing – review & editing, Supervision, Conceptualization.

Declaration of competing interest

The authors declare that they have no known competing financial interests or personal relationships that could have appeared to influence the work reported in this paper.

Data availability

Data will be made available on request.

Acknowledgments

Financial support (grant number: MESM_P42748) from the Aviation Industry Corporation of China (AVIC) Manufacturing Technology Institute (MTI) is gratefully acknowledged.

For the purpose of open access, the authors have applied a Creative Commons Attribution (CCBY) licence to any Author Accepted Manuscript version arising.

References

[1] J. Munroe, K. Wilkins, M. Gruber, M.S. Domack, Integral airframe structures (IAS): Validated feasibility study of integrally stiffened metallic fuselage panels for reducing manufacturing costs, 2000.

[2] A.C.L. Lam, Z. Shi, H. Yang, L. Wan, C.M. Davies, J. Lin, S. Zhou, Creep-age forming AA2219 plates with different stiffener designs and pre-form age conditions: Experimental and finite element studies, J. Mater Process. Technol. 219 (2015) 155–163, http://dx.doi.org/10.1016/j.jmatprotec.2014.12.012.

[3] L. Zhan, J. Lin, T.A. Dean, M. Huang, Experimental studies and constitutive modelling of the hardening of aluminium alloy 7055 under creep age forming conditions, Int. J. Mech. Sci. 53 (2011) 595–605, http://dx.doi.org/10.1016/j.ijmecsci.2011.05.006.

[4] Y. Yang, L. Zhan, Forming characteristics of AA2219 integrally-stiffened plate subjected to creep age forming, Procedia Manuf. 15 (2018) 1000–1007, http://dx.doi.org/10.1016/J.PROMFG.2018.07.394.

[5] Y. Yang, L. Zhan, R. Shen, J. Liu, X. Li, M. Huang, D. He, Z. Chang, Y. Ma, L. Wan, Investigation on the creep-age forming of an integrally-stiffened AA2219 alloy plate: experiment and modeling, Int. J. Adv. Manuf. Technol. 95 (2018) 2015–2025, http://dx.doi.org/10.1007/s00170-017-1248-3.

[6] L. Zhan, J. Lin, T.A. Dean, A review of the development of creep age forming: Experimentation, modelling and applications, Int. J. Mach. Tools Manuf. 51 (2011) 1–17, http://dx.doi.org/10.1016/j.ijmachtools.2010.08.007.

[7] F. Lyu, Y. Li, X. Huang, Z. Shi, Y. Zeng, J. Lin, An investigation of creep age forming of AA7B04 stiffened plates: Experiment and FE modelling, J. Manuf. Process. 37 (2019) 232–241, http://dx.doi.org/10.1016/J.JMAPRO.2018.11.031.

[8] Y. Yan, M. Wan, H. Wang, Prediction of stiffener buckling in press bend forming of integral panels, Trans. Nonferrous Met. Soc. China 21 (2011) 2459–2465, http://dx.doi.org/10.1016/S1003-6326(11)61037-6.

[9] W. Zhou, Q. Rong, Z. Shi, Y. Zeng, Non-linear finite element investigation of formability limit by buckling in creep age forming of stiffened panels, Procedia Manuf. 50 (2020) 625–629, http://dx.doi.org/10.1016/j.promfg.2020.08.112.

[10] W. Zhou, Z. Shi, Q. Rong, X. Bai, Y. Zeng, J. Lin, Experimental and numerical investigations on buckling behaviour of stiffened panel during creep age forming, Thin-Walled Struct. 172 (2022) 108940, http://dx.doi.org/10.1016/j.tws.2022.108940.

[11] M.A. Bessa, S. Pellegrino, Design of ultra-thin shell structures in the stochastic post-buckling range using Bayesian machine learning and optimization, Int. J. Solids Struct. 139–140 (2018) 174–188, http://dx.doi.org/10.1016/J.IJSOLSTR.2018.01.035.

[12] K. Tian, Z. Li, J. Zhang, L. Huang, B. Wang, Transfer learning based variable-fidelity surrogate model for shell buckling prediction, Compos. Struct. 273 (2021) 114285, http://dx.doi.org/10.1016/J.COMPSTRUCT.2021.114285.

[13] C. Bisagni, R. Vescovini, Analytical formulation for local buckling and post-buckling analysis of stiffened laminated panels, Thin-Walled Struct. 47 (2009) 318–334, http://dx.doi.org/10.1016/J.TWS.2008.07.006.

[14] A. Rahbar-Ranji, Elastic buckling analysis of longitudinally stiffened plates with flat-bar stiffeners, Ocean Eng. 58 (2013) 48–59, http://dx.doi.org/10.1016/j.oceaneng.2012.09.018.

[15] J.K. Paik, A.K. Thayamballi, Buckling strength of steel plating with elastically restrained edges, Thin-Walled Struct. 37 (2000) 27–55, http://dx.doi.org/10.1016/S0263-8231(00)00009-4.

[16] W. Zhou, Y. Li, Z. Shi, J. Lin, An analytical solution for elastic buckling analysis of stiffened panel subjected to pure bending, Int. J. Mech. Sci. 161–162 (2019) 105024, http://dx.doi.org/10.1016/J.IJMECSCI.2019.105024.

[17] W. Zhou, Z. Shi, Y. Li, Q. Rong, Y. Zeng, J. Lin, Elastic–plastic buckling analysis of stiffened panel subjected to global bending in forming process, Aerosp. Sci. Technol. 115 (2021) 106781, http://dx.doi.org/10.1016/j.ast.2021.106781.

[18] T. Manco, J.P. Martins, C. Rigueiro, L. Simões da Silva, Semi-analytical orthotropic model for the prediction of the post-buckling behaviour of stiffened cylindrically curved steel panels under uniaxial compression, Comput. Struct. 211 (2019) 27–42, http://dx.doi.org/10.1016/J.COMPSTRUC.2018.08.015.

[19] R. Li, X. Zheng, H. Wang, S. Xiong, K. Yan, P. Li, New analytic buckling solutions of rectangular thin plates with all edges free, Int. J. Mech. Sci. 144 (2018) 67–73, http://dx.doi.org/10.1016/J.IJMECSCI.2018.05.041.

[20] M. Kadkhodayan, M. Maarefdoust, Elastic/plastic buckling of isotropic thin plates subjected to uniform and linearly varying in-plane loading using incremental and deformation theories, Aerosp. Sci. Technol. 32 (2014) 66–83, http://dx.doi.org/10.1016/J.AST.2013.12.003.

[21] H. BeikMohammadlou, H. EkhteraeiToussi, Parametric studies on elastoplastic buckling of rectangular FGM thin plates, Aerosp. Sci. Technol. 69 (2017) 513–525, http://dx.doi.org/10.1016/J.AST.2017.07.015.

[22] Y.L. Guo, J. Lindner, Analysis of elastic–plastic interaction buckling of stiffened panels by spline finite strip method, Comput. Struct. 46 (1993) 529–536, http://dx.doi.org/10.1016/0045-7949(93)90222-Y.

[23] L. Rønning, O.S. Hopperstad, P.K. Larsen, Numerical study of the effects of constitutive models on plastic buckling of plate elements, Eur. J. Mech. A 29 (2010) 508–522, http://dx.doi.org/10.1016/j.euromechsol.2010.02.001.

[24] J. Becque, The application of plastic flow theory to inelastic column buckling, Int. J. Mech. Sci. 111–112 (2016) 116–124, http://dx.doi.org/10.1016/j.ijmecsci.2016.04.005.

[25] M. Maarefdoust, M. Kadkhodayan, Elastoplastic buckling analysis of rectangular thick plates by incremental and deformation theories of plasticity, J. Aerosp. Eng. 229 (7) (2015) 1280–1299, http://dx.doi.org/10.1177/0954410014550047.

[26] X. Kong, Y. Yang, J. Gan, T. Yuan, L. Ao, W. Wu, Experimental and numerical investigation on the detailed buckling process of similar stiffened panels subjected to in-plane compressive load, Thin-Walled Struct. 148 (2020) 106620, http://dx.doi.org/10.1016/j.tws.2020.106620.

[27] T. Yuan, Y. Yang, X. Kong, W. Wu, Similarity criteria for the buckling process of stiffened plates subjected to compressive load, Thin-Walled Struct. 158 (2021) 107183, http://dx.doi.org/10.1016/j.tws.2020.107183.

[28] Y. Wang, P. Qiao, Postbuckling analysis of orthogonally-stiffened plates by a simplified spline finite strip method, Thin-Walled Struct. 166 (2021) 108122, http://dx.doi.org/10.1016/J.TWS.2021.108122.

[29] Y. Xu, Y. Tong, M. Liu, B. Suman, A new effective smeared stiffener method for global buckling analysis of grid stiffened composite panels, Compos. Struct. 158 (2016) 83–91, http://dx.doi.org/10.1016/J.COMPSTRUCT.2016.09.015.

[30] D. Wang, M.M. Abdalla, Global and local buckling analysis of grid-stiffened composite panels, Compos. Struct. 119 (2015) 767–776, http://dx.doi.org/10.1016/J.COMPSTRUCT.2014.09.050.

[31] E. Wodesenbet, S. Kidane, S.S. Pang, Optimization for buckling loads of grid stiffened composite panels, Compos. Struct. 60 (2003) 159–169, http://dx.doi.org/10.1016/S0263-8223(02)00315-X.

[32] M.B. Francisco, J.L.J. Pereira, G.A. Oliver, F.H.S. da Silva, S.S. da Cunha, G.F. Gomes, Multiobjective design optimization of CFRP isogrid tubes using sunflower optimization based on metamodel, Comput. Struct. 249 (2021) http://dx.doi.org/10.1016/J.COMPSTRUC.2021.106508.

[33] B. Wang, K. Tian, P. Hao, Y. Zheng, Y. Ma, J. Wang, Numerical-based smeared stiffener method for global buckling analysis of grid-stiffened composite cylindrical shells, Compos. Struct. 152 (2016) 807–815, http://dx.doi.org/10.1016/J.COMPSTRUCT.2016.05.096.

[34] O.F. Hughes, M. Ma, Elastic tripping analysis of asymmetrical stiffeners, Comput. Struct. 60 (1996) 369–389, http://dx.doi.org/10.1016/0045-7949(95)00389-4.

[35] M. Fujikubo, T. Yao, Elastic local buckling strength of stiffened plate considering plate/stiffener interaction and welding residual stress, Mar. Struct. 12 (1999) 543–564.

[36] T.X. Yu, Z. Liangchi, Plastic Bending: Theory and Applications, World Scientific, 1996.

[37] L. Bai, M.A. Wadee, A. Köllner, J. Yang, Variational modelling of local–global mode interaction in long rectangular hollow section struts with Ramberg–Osgood type material nonlinearity, Int. J. Mech. Sci. 209 (2021) 106691, http://dx.doi.org/10.1016/J.IJMECSCI.2021.106691.

[38] E. Ruocco, Elastic/plastic buckling of moderately thick plates and members, Comput. Struct. 158 (2015) 148–166, http://dx.doi.org/10.1016/J.COMPSTRUC.2015.06.007.

[39] W. Zhang, X. Wang, Elastoplastic buckling analysis of thick rectangular plates by using the differential quadrature method, Comput. Math. Appl. 61 (2011) 44–61, http://dx.doi.org/10.1016/J.CAMWA.2010.10.028.

[40] E. Hasrati, R. Ansari, H. Rouhi, Elastoplastic postbuckling analysis of moderately thick rectangular plates using the variational differential quadrature method, Aerosp. Sci. Technol. 91 (2019) 479–493, http://dx.doi.org/10.1016/j.ast.2019.05.043.

[41] H. Zhong, C. Gu, Buckling of simply supported rectangular Reissner–Mindlin plates subjected to linearly varying in-plane loading, J. Eng. Mech. 132 (2006) 578–581, http://dx.doi.org/10.1061/(asce)0733-9399(2006)132:5(578).

[42] S.P. Timoshenko, J.M. Gere, Theory of Elastic Stability, McGraw-Hill, New York, 1961.

[43] Q. Rong, Z. Shi, Y. Li, J. Lin, Constitutive modelling and its application to stress-relaxation age forming of AA6082 with elastic and plastic loadings, J. Mater Process. Technol. 295 (2021) 117168, http://dx.doi.org/10.1016/J.JMATPROTEC.2021.117168.

[44] X. Wang, J. Huang, Elastoplastic buckling analyses of rectangular plates under biaxial loadings by the differential qudrature method, Thin-Walled Struct. 47 (2009) 14–20, http://dx.doi.org/10.1016/j.tws.2008.04.006.